Anharmonic Calculations of Vibrational Spectra for Molecular Adsorbates: A Divide-and-Conquer Semiclassical Molecular Dynamics Approach

Marco Cazzaniga,[1, a)] Marco Micciarelli,[1] Francesco Moriggi,[1] Agnes Mahmoud,[1] Fabio Gabas,[1] and Michele Ceotto[1, b)]

Dipartimento di Chimica, Università degli Studi di Milano, via Golgi 19, 20133 Milano, Italy.

Vibrational spectroscopy of adsorbates is becoming an important investigation tool for catalysis and material science. This paper presents a semiclassical molecular dynamics method able to reproduce the vibrational energy levels of systems composed by molecules adsorbed on solid surfaces. Specifically, we extend our divide-and-conquer semiclassical method for power spectra calculations to gas-surface systems and interface it with plane-wave electronic structure codes. The Born-Oppenheimer classical dynamics underlying the semiclassical calculation is full dimensional and our method includes not only the motion of the adsorbate but also those ones of the surface and the bulk. The vibrational spectroscopic peaks related to the adsorbate are accounted together with the most coupled phonon modes to obtain spectra amenable to physical interpretations. We apply the method to the adsorption of CO, NO and H_2O on anatase-TiO_2 (101) surface. We compare our semiclassical results with the single-point harmonic estimates and the classical power spectra obtained from the same trajectory employed in the semiclassical calculation. We find that CO and NO anharmonic effects of fundamental vibrations are similarly reproduced by the classical and semiclassical dynamics, and that H_2O adsorption is fully and properly described in its overtone and combination band relevant components only by the semiclassical approach.

[a)]Electronic mail: marco.cazzaniga@unimi.it

[b)]Electronic mail: michele.ceotto@unimi.it

I. INTRODUCTION

Quantum nuclear effects are ubiquitous in molecular mechanics, even if most of the computational methods *en vogue* treat nuclei as classical particles. The main justification for this choice would be that nuclear quantum effects wash out, even for the light hydrogen atom, especially in condensed phase systems. In this paper we focus on molecular adsorbate spectroscopy and show when molecular adsorbates can be reasonably treated with classical mechanics, and when it is necessary to include nuclear quantum effects to obtain a more complete and realistic picture.

To this end we need, on one side, theoretical methods capable of classical and quantum simulations, on the other experimental results allowing for a direct quantitative comparison. Infrared (IR) and Raman spectroscopy of adsorbates offer this field of comparison.[1–4] Given the many electrons and nuclei involved, the state of the art of computational tool for vibrational spectroscopy of adsorbate molecules is represented by the harmonic approximation, i.e. the Hessian diagonalization at the Born-Oppenheimer (BO) equilibrium geometry. Even if some authors overcome this limitation by including anharmonicities by means of the classical velocity-velocity correlation function,[5–8] semiempirical Hamiltonians,[9] or perturbation theories,[10] we think that it is important to include quantum mechanical effects for a better understanding of the experimental results. Therefore, we decided to extend the Divide-and-Conquer Semiclassical Initial Value Representation (DC SCIVR) method,[11] a quantum mechanical approach recently developed in our group, to the calculation of the vibrational power spectra of molecular adsorbates. This semiclassical (SC) method is based on classical trajectories and it has proved to include nuclear quantum mechanical effects quite accurately. It is implementable both on analytical potential energy surfaces (PESs) and on a direct ab initio molecular dynamics, i.e. on-the-fly, approach. More specifically, we will extend DC SCIVR from isolated molecular system spectroscopy calculations to molecules adsorbed on surfaces, including the vibrational contributions of the surface and the bulk, and without any *ad hoc* decoupling. DC SCIVR can selectively provide the peaks of the spectrum that are related to the adsorbate vibrations, including those of the surface and the bulk, because it is based on full dimensional classical trajectories.[12,13]

The importance of developing nuclear quantum mechanic tools for adsorption studies has been already stressed both from experimental and theoretical results, especially on metallic

substrates and for organic adsorbates.[14–24] In particular for theoretical spectroscopic investigation beyond the harmonic approximation, efforts have been dedicated to water adsorption on Pd(111).[10] Here we choose to focus on the investigation of molecular adsorption phenomena not only for the intrinsic interest in this fundamental phenomena but also for the several technological and industrial applications. Indeed, transition metal oxide surfaces can be appealing systems to drive photo-catalytic processes, especially in the field of catalysis of pollutant degradation photoinduced reactions[25] and hydrogen generation[26,27] processes, which have been receiving great attention as they may help in solving serious environmental and energy challenges. Among all the possible choices for materials with photo-catalytic properties, titanium dioxide (TiO_2) is considered one of the most promising semiconductor materials because of its strong photo-oxidative ability, its low cost, non-toxicity and chemical stability.[28–35] Many open issues concerning the surface-pollutant interactions and the structure-property relationship are still unsolved and progresses in this regard may be very useful. In particular, the shifts of the vibrational frequencies of the molecule itself compared to the gas phase, both thanks to IR and Raman measurements and theoretical predictions,[36,37] is a powerful tool for a better understanding of the mechanisms involved in the interaction between a surface and an adsorbed molecule, and the observed photochemical processes. In this paper, we will show the vibrational spectra of CO, NO and H_2O, adsorbed on the anatase-TiO_2(101) surface, which is the most thermodynamically stable anatase surface. These molecules have been extensively tested with spectroscopic experiments and they represent a typical benchmark.[38]

The paper is organized as follow. Section II is divided into three parts: The first one reviews the DC-SCIVR method, the second implements DC SCIVR for adsorbate spectroscopic calculations, and the final one describes the computational setup. In Section III our results are reported. These are divided into geometry considerations, vibrational spectra calculations and adsorbate-surface coupling studies. Finally Section IV concludes the paper.

II. METHODS

In this section we present the theoretical implementations of semiclassical molecular dynamics for the calculation of spectra of molecular adsorbates. We first briefly review the theory of the DC-SCIVR method, introduced by one of us. A more extended presentation

of this semiclassical method can be found elsewhere.[12,39] Then, we will describe how we can implement this formalism for spectroscopic calculations of molecules adsorbed on surfaces. The method is able to account for the quantum dynamical effects of the surface and part of the bulk in the molecular vibrational spectra. Here, we will calculate nuclear power spectra. However, the same formalism can be promptly extended for the calculation of any kind of nuclear motion related type of spectra. At the end, the details of the computational set-up are described.

The vibrational frequencies of a quantum system governed by the Hamiltonian $\hat{H}$, can be accessed through the quantum power spectrum $I(E)$, which is given by the Fourier transform of the survival amplitude[40] of an arbitrary reference state $|\chi\rangle$

$$I\left(E\right) \equiv \frac{1}{2\pi\hbar} \int_{+\infty}^{-\infty} \left\langle \chi \left| e^{-i\hat{H}t/\hbar} \right| \chi \right\rangle e^{iEt/\hbar} dt. \tag{1}$$

We perform the quantum dynamics evolution in Eq. (1) using the semiclassical (SC) molecular dynamics, which can be derived by a stationary phase approximation of the Feynman Path Integral propagator for the quantum time-evolution operator $e^{-i\hat{H}t/\hbar}$.[41,42] In other words, the SC propagator is composed of all the trajectories starting from a given position $\mathbf{q}\left(0\right)$ and ending to a given one $\mathbf{q}\left(t\right)$ in a fixed t amount of time. This boundary values problem[43–46] has been made amenable to computational simulations only with the reformulation of the semiclassical propagator in terms of initial conditions $\left(\mathbf{p}\left(0\right), \mathbf{q}\left(0\right)\right)$. The Semiclassical Initial Value Representation (SCIVR) has been originally proposed by Miller, and later implemented by several authors.[40,42,45,47–61] For spectroscopic calculations, it has been found convenient to introduce a time averaging filter, the so called TA-SCIVR,[62–64] in addition to the phase space integration introduced by the IVR approach. More specifically, after exchanging the phase integral with the additional time integration, it results that a much smaller number of IVR trajectories are necessary for numerical convergence. This formulation still needs an order of a thousand trajectories per degree of freedom for reaching numerical convergence. Later, the Multiple Coherent formulation of SCIVR (MC SCIVR) was introduced by one of us, where only a few tailored trajectories are necessary. This implementation of the SCIVR opened the route to on-the-fly semiclassical simulations.[65–70]

In the MC SCIVR formulation, the power spectrum is given by

$$I(E) = \frac{1}{N_{traj}} \sum_{i=1}^{N_{traj}} \frac{1}{2\pi\hbar T} \left| \int_0^T e^{\frac{i}{\hbar}[S_t(\mathbf{p}_i(0),\mathbf{q}_i(0))+Et+\phi_t]} \langle \chi | \mathbf{p}_i(t), \mathbf{q}_i(t) \rangle dt \right|^2 \quad (2)$$

where T is the total simulation time, $S_t(\mathbf{p}(0), \mathbf{q}(0))$ is the classical action, ϕ_t indicates the phase of the Herman-Kluk pre-exponential factor $C_t(\mathbf{p}(0), \mathbf{q}(0))$

$$C_t(\mathbf{p}(0), \mathbf{q}(0)) = \\ = \sqrt{\det \left| \frac{1}{2} \left(\mathbf{M_{qq}} + \Gamma^{-1}\mathbf{M_{pp}}\Gamma - i\hbar\Gamma\mathbf{M_{qp}} + \frac{i\Gamma^{-1}}{\hbar}\mathbf{M_{pq}} \right) \right|}, \quad (3)$$

and $|\mathbf{p}(t), \mathbf{q}(t)\rangle$ is a coherent state of the type:[40,49,55,71–73]

$$\langle \mathbf{x} | \mathbf{p}(t), \mathbf{q}(t) \rangle = \left(\frac{\det(\Gamma)}{\pi^F} \right)^{1/4} \\ e^{-(\mathbf{x}-\mathbf{q}(t))^T\Gamma(\mathbf{x}-\mathbf{q}(t))/2 + i\mathbf{p}^T(t)(\mathbf{x}-\mathbf{q}(t))/\hbar}. \quad (4)$$

In Eq.s (3) and (4) Γ is a diagonal width matrix for bound state calculations, with coefficients usually equal to the square root of the harmonic vibrational frequencies. In addition, the time evolution of Eq. (3) is performed by evolving the equations of motion of the monodromy matrix elements[74] of the type $\mathbf{M}_{ij} = \partial\mathbf{i}(t)/\partial\mathbf{j}(0)$, which requires the knowledge of the Hessian of the potential along each trajectory. This is actually the most computationally expensive part of the evaluation of semiclassical spectra and several numerical implementations have been introduced to ease this bottleneck.[75–79] In few words, the MC SCIVR approach is based on the assumption that a suitable choice of a single or few trajectories, each one associated to a reference state, can still yield accurate vibrational frequencies. More specifically, each trajectory is initialized such that its energy is close to a given quantum vibrational eigenvalue. Since the exact eigenvalues are unknown, a good strategy is to evolve the trajectories starting from the equilibrium atomic coordinates ($\mathbf{q}_{\text{eq}}$) and with a corresponding momentum provided by the harmonic estimate ($\mathbf{p}^2_{\text{eq}}/2m = \hbar\boldsymbol{\omega}(\mathbf{n} + 1/2)$) of the vibrational eigenvalue. In addition, one can select spectroscopic peaks by using reference

state combinations of the type:

$$|\chi\rangle = |\mathbf{p}_{\mathrm{eq}}, \mathbf{q}_{\mathrm{eq}}\rangle + \boldsymbol{\gamma}\,|-\mathbf{p}_{\mathrm{eq}}, \mathbf{q}_{\mathrm{eq}}\rangle \tag{5}$$

where $\boldsymbol{\gamma}$ is a vector such that when all its elements are equal to 1, the ZPE peak and even overtone spectroscopic signals are enhanced.[68] Instead, by switching one of its component to -1, the fundamental and the odd overtones of that mode component are enhanced. This approach has been shown to provide quite accurate results when compared to exact quantum mechanical simulations.[70,80–89]

Divide-and-Conquer Semiclassical Molecular Dynamics

Despite the aforementioned implementations to semiclassical dynamics for high dimensional applications, systems with a large number of degrees of freedom remain unfeasible, not only because of the curse of dimensionality, but also because it becomes difficult to resolve the spectroscopic signals. For these reasons, we recently proposed a "Divide and Conquer" strategy[11–13] based on the idea of obtaining the power spectrum $I(E)$ of Eq. (1) as composition of partial spectra $\widetilde{I}(E)$ computed in an M-dimensional subspace of the full N_{vib}-dimensional space. The resulting expression for the power spectrum is the following:

$$\widetilde{I}(E) = \frac{1}{2\pi\hbar T}\frac{1}{N_{traj}}\sum_{i=1}^{N_{traj}} \left|\int_0^T e^{\frac{i}{\hbar}\left[\tilde{S}_t(\tilde{\mathbf{p}}_i(0),\tilde{\mathbf{q}}_i(0))+Et+\tilde{\phi}_t\right]}\langle\tilde{\chi}|\tilde{\mathbf{p}}_i(t),\tilde{\mathbf{q}}_i(t)\rangle dt\right|^2 \tag{6}$$

where all the quantities with the tilde superscript are projected in the M-subspace, by a singular value decomposition, with the consequent dimensional reduction for the semiclassical calculation. While most of the quantities in Eq. (6) can be directly projected starting from the full dimensional one, this is not true for the classical action $\tilde{S}_t$, due to the non separability of the potential energy term. Therefore the following expression for the projected potential has been introduced

$$\tilde{V}_S(\tilde{\mathbf{q}}_M(t)) = V(\tilde{\mathbf{q}}_M(t);\mathbf{q}_{N_{vib}-M}(t)) - V(\mathbf{q}_M^{eq};\mathbf{q}_{N_{vib}-M}(t)) \tag{7}$$

where the effect of the degrees of freedom outside the M-subspace is subtracted from the full dimensional potential after fixing the M-subspace variables at their equilibrium geometry $\mathbf{q}_M^{eq}$. This approximation is as much as better the M-subspace oscillations are nearby the equilibrium. Also eq. (7) is the exact projected potential in the separable limit. The subspaces are chosen such that strongly coupled modes are included in the same subspace. There are different approaches to settle the subspaces, as reported in details in Refs. 39 and 12. In Sec. II we will describe in details the one we adopt in this work.

Eq. (6) is our working DC SCIVR formula and it provides the quantum power spectrum. For comparison and for a better understanding of the importance of including quantum effects in nuclear dynamics simulations, we calculate the classical equivalent of Eq. (6) as well. This is the classical power spectrum, i.e. the Fourier transform of the velocity correlation function, which is equal to

$$\widetilde{I}_{qcl}(E) = \frac{1}{2\pi\hbar T}\int_0^T dt e^{\frac{i}{\hbar}Et} \times \left(\frac{1}{2\pi\hbar}\right)^M \int\int d\tilde{\mathbf{p}}(0)\, d\tilde{\mathbf{q}}(0)\, \tilde{\mathbf{p}}(t)\, \tilde{\mathbf{p}}(0) \tag{8}$$

In the following we denote this approximation as the "quasi-classical" one, because each trajectory has an energy equal to each vibrational energy level. Instead, classical power spectra are usually obtained from NVE trajectories previously thermostated with a NVT procedure. At zero Kelvin, the classical power spectra becomes the harmonic approximation and it can not be employed as a term of comparison with our DC SCIVR results, which are zero Kelvin spectra. In each simulation, we keep the length of the trajectory fixed to 2500 time-steps of 10 a.u. each.

Extension of DC SCIVR for Adsorbant-Surface Spectroscopy

The dimensionality of a typical adsorbant-surface system is at least of the order of hundreds of degrees of freedom. A full dimensional SC calculation is unfeasible, even with the few classical trajectories required by the MC SCIVR approach, and the DC SCIVR method described above becomes mandatory. Before applying DC SCIVR to the problem of surface-adsorbed molecules, we need first to put in place some considerations. The full spectrum of the system that describes the adsorption of a molecule is composed of bulk and surface vibra-

tions (phonons) plus the adsorbate vibrations. Most of these vibrational motions are strictly related to the bulk and are not necessary for the understanding of the adsoprtion process. For this reason, the Divide-and-Conquer strategy helps in this case to bypass the complexity of the system by calculating the Hessian components only for the subspaces where the vibrational modes of the adsorbate are involved, and not the full dimensional Hessian or the Hessian for other entirely phononic subspaces. However, the classical dynamics is always full dimensional and fully coupled, i.e. the BO surface remains the exact one. One can naively focus only on a subspace of the vibrational modes that is composed exclusively of adsorbate modes. This choice is quite limiting and it does not take into account properly of the surface role. Instead, we prefer to adopt the approach called "Hessian space-decomposition method", introduced in Ref. 12. To summarize, this method starts from the evaluation of the coupling strength between modes in terms of the averaged Hessian off-diagonal elements $\bar{H}_{ij}$ obtained from absolute values of the Hessian matrix in normal mode coordinates over the trajectory steps: $\bar{H}_{ij} = \sum_{k=1}^{N} |H_{ij}|/N$. After fixing a given threshold value ϵ, we divide the modes in subspaces by setting all the averaged coupling elements that are smaller than ϵ equal to zero, i.e.

$$\bar{H}_{ij} = \begin{cases} \bar{H}_{ij} & \text{if } \left|\bar{H}_{ij}\right| \geq \epsilon \\ 0 & \text{if } \left|\bar{H}_{ij}\right| < \epsilon \end{cases} . \tag{9}$$

The resulting block-diagonal matrix defines the subspaces. In other words, if mode i and mode j are such that $\left|\bar{H}_{ij}\right| \geq \epsilon$, they are enrolled on the same subspace. When $\left|\bar{H}_{ij}\right| < \epsilon$ and there exits a third mode k such that $\left|\bar{H}_{ik}\right| \geq \epsilon$ and/or $\left|\bar{H}_{kj}\right| \geq \epsilon$, i and j are still enrolled on the same vibrational subspace, otherwise not. The drawback of this approach is that ϵ is an arbitrary parameter, and smaller values would correspond to larger subspace dimensions. Since it is not possible to choose a priori a suitable value of ϵ, we tested different choices, in a way to compromise between good quality spectra and subspace dimensionality suitable for numerical convergence. For the Hessian averaging, one would need the value of the full Hessian matrix at each trajectory step. This is computationally prohibitive in the present case, given the large dimension of the system composed by the adsorbate, the surface and the bulk. Thus, our choice has been to apply the averaged-Hessian approach only on a limited number of time-steps uniformly distributed along the trajectory. To sum up, we perform full dimensional classical dynamics. Then, we partition the modes into groups using full dimensional Hessian calculations. Finally, we calculated the spectrum of each group of

modes separately using reduced dimensionality semiclassical quantities as in Eq.(6).

To prove that a normal mode subdivision based on a small number of full dimensional Hessian matrices is still reliable, we report a benchmark test for the glycine molecule. Thanks to its manageable size, this molecule allows us to validate the partial Hessian normal modes partition described above in comparison to a subdivision into subspaces, where the full dimensional Hessian has been calculated at each time-step and the case of the full 24-dimensional MC SCIVR calculation without any divide-and-conquer approximation.[81] The same computational setup employed in Ref. 81 is employed here. A 2500 time-steps trajectory (0.6 ps) is evolved using the DFT B3LYP functional, in conjunction with the aVDZ basis set, as implemented in the NWChem package of software.[90] Here, we focus our attention only on the asymmetric and symmetric NH_2 stretching modes as if they were the adsorbate modes, for which we have the evidence of a non-negligible coupling with the other degrees of freedom by inspection of the off-diagonal Hessian elements. In particular, we perform a subdivision based on the average over both of all the 2500 Hessian matrices calculated step by step along the trajectory and on the evaluation of 20 Hessians only. We take as a reference the 16-dimensional subspace coming from the Hessian averaged on 2500 steps and obtained with threshold value equal to $\epsilon = 2 \times 10^{-6}$, and perform different vibrational space subdivisions using different ϵ values for the 20 steps averaged Hessian. The most crude choice is a bidimensional subspace, where only the two NH stretch motions are included. The corresponding spectrum is reported in panel (a) of Fig. 1 and no clear assignment is possible for this spectrum. By gradually increasing the dimensionality of the NH subspace, the stretching peaks gradually appear more and more well-defined. When using the same ϵ value equal to 2×10^{-6} both for the 20 and 2500 Hessian evaluations, we obtain two different 16-dimensional subspaces for the NH stretches, which differ for three normal modes. However, the spectroscopic signal for the two NH stretches are identical. This proves that when the subspace is large enough, (i) the results are converged and (ii) one can use only 20 Hessians instead of 2500. Eventually, it is not necessary to perform higher dimensional calculations if one is interested in these modes only. The criteria for understanding if the subspace is large enough are both qualitative and quantitative. The quality of the spectrum is increased when the ZPE and fundamental peaks present small intensity side peaks and there are no peaks at lower energy than the ZPE one. The quantitative criterion is satisfied when, by increasing the dimensionality of the subspace, the position and the intensity of

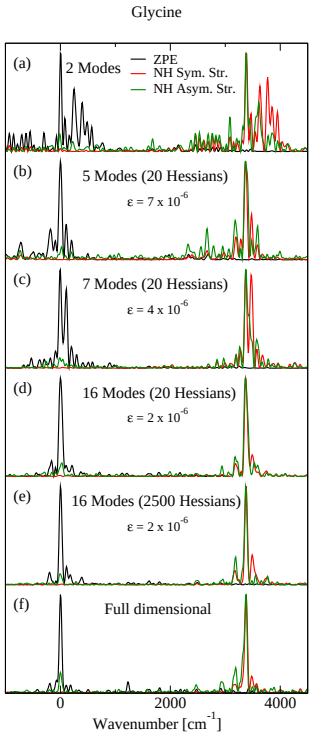

Figure 1. Semiclassical glycine NH_2 stretching peaks with different vibrational space subdivisions strategies. The spectra have been shifted with the ZPE peak to 0 energy value.

the peaks with respect to the ZPE one do not change. In conclusions, we introduce a different procedure respect to our previous DC SCIVR one. The main differences are that (i) the subspace subdivision is calculated with much fewer Hessian evaluations, (ii) the power spectrum is calculated only for the subspaces containing the adsorbate vibrational normal mode peaks, and (iii) only the projected potential and the Hessian sub-block of interest are calculated during the dynamics.

We believe that this strategy can be applied to any complex system where the spectroscopic signal of only a part of the system is of interest. In the following we will apply it to the specific case of the adsorbate-surface system, where mainly the spectroscopic signal of the molecule is of interest and part of the bulk phonon peaks are superfluous.

Computational details

To simulate the dynamics of the adsorbate-surface system we employ the open source Quantum-Espresso (Q-E)[91,92] suite of programs. All calculations are performed using ultra-

soft pseudopotentials with energy cutoff for the wavefunction of 40 Ry for the adsorption of CO, of 60 Ry for the adsorption of NO, and 40 Ry for the adsorption of H_2O (the corresponding cutoff for the density is set to 400 Ry for CO, 480 Ry for NO, and 400 Ry for H_2O). The Brillouin zone was sampled using the Γ point only. Because of the unpaired electron in NO, we performed a spin polarized simulation to describe its adsorption, while the simulations for CO and H_2O adsorption are unpolarized. The supercell used to describe the surface has been generated by cutting a bulk with atomic coordinates obtained by a TiO_2 anatase bulk geometry at the theoretical lattice constants, i.e. by cutting the bulk along the plane defined by the chosen Miller indexes with atomic coordinates at the DFT lattice parameters. We choose the (101) facet because it is the thermodynamically most stable one. The adsorption geometries were determined by a relaxation of the atoms of the surfaces and the adsorbates. Out of the four Ti layers, the two deepest layers were frozen to the bulk atomic positions, while the others are free to relax to their equilibrium geometry. A separation between periodic replica of the slabs has been achieved by inserting around 10 Å of vacuum for CO, 9 Å for NO and 10 Å for H_2O. The surface model presents 4 Ti_{5c} sites available for adsorption with one adsorbed molecule per unit cell corresponding to a coverage $\Theta = 0.25$ monolayer, as shown in Fig. 2. These atomic coordinates represent the starting atomic configuration for the evaluation of the equilibrium Hessian matrix, and for the successive trajectory simulations. The presence of the fixed layers in the slab causes the starting geometry not to be a full-dimensionality slab minimum of the PES for the entire simulation cell. In addition, to avoid the subspace analysis to provide a coupling with modes involving fixed atoms, we set to infinity the masses of the fixed slab atoms and consequently their Hessian component are equal to zero. Also, the resulting matrix will be used throughout the whole simulation to convert the Cartesian coordinates to normal modes.

Since we choose to work with a PBE functional and keep a minimal level of convergence of the simulations, we checked the adequacy of our surface model (referred hereafter as Q-E_f - fast) for the CO and NO by comparing the equilibrium geometries and the binding energies against two calculations performed with more accurate DFT levels. For these references we choose an hybrid functional (PBE0) and a PBE+U calculation. The PBE0 results have been performed with the all-electron localized Gaussian basis sets as available in the CRYSTAL code (referred as CRYSTAL).[93,94] We fix the thresholds for the truncation

(a) CO @ Anatase(101)

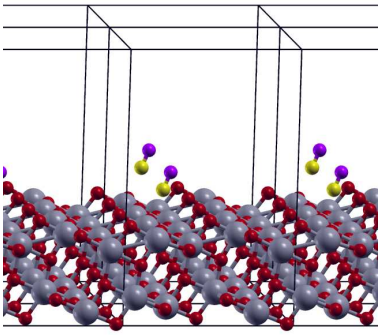

(b) NO @ Anatase(101)

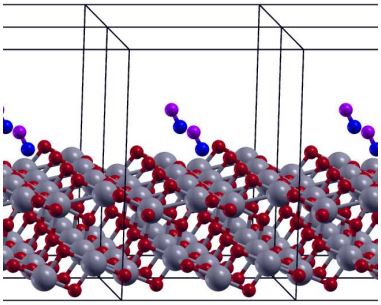

(c) H_2O @ Anatase(101)

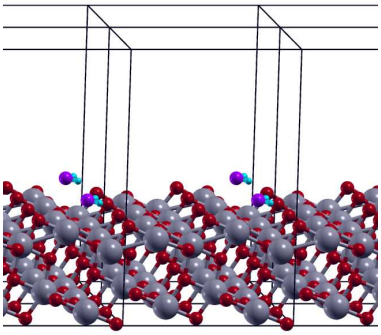

Figure 2. Optimized geometries of CO (panel (a)), NO (panel (b)) and H_2O (panel (c)) adsorbed on the TiO_2 anatase (101) surface. Ti atoms are in gray, surface Oxygen in red, while molecular Oxygen in violet. Carbon atoms in yellow, Nitrogen in blue and Hydrogen in cyan.

of infinite lattice sums T1 = T2 = T3 = 10^{-7} a.u., T4 = 10^{-14} a.u. and T5 = 10^{-20} a.u. The convergence threshold for the SCF energy is set to 10^{-8} Ha. Reciprocal space is sampled according to a sub-lattice with a shrinking factor equals to 6, i.e. $6 \times 6 \times 1$ Monkhorst-Pack net. Since periodicity should not be guaranteed for CRYSTAL local atomic orbitals, we build a 2d periodic slab scheme and the model is a real two-dimensional system, where periodicity (and Bloch theorem conditions as well) is lost in the direction perpendicular

to the crystallographic plane. The dimension of the 2d periodic slab is a 2×1 supercell with respect to the primitive cell. The second higher level calculations have been performed with the Q-E suite (referred as Q-E_i - intense), where the kinetic energy cutoff for wave functions equal to 40 Ry. The convergence threshold for the PWScf energy was set to 10^{-7} Ry. A 2×1 supercell with respect to the conventional cell was arranged with a reciprocal space k-points grid equals to $6 \times 6 \times 1$, and a value for the Hubbard U equal to U = 3.3 eV. An overall comparison for the anatase-TiO_2 lattice constants is reported in Table S1 of the Supplementary Information (SI). The Binding Energy (BE) reported below has been calculated using the following expression

$$\mathrm{BE} = -\frac{E_{sys} - (E_{slab} + nE_{ads})}{n} \tag{10}$$

where E_{slab} is the energy of the slab, E_{ads} is the energy of the isolated adsorbant molecule in its equilibrium configuration, n is the number of adsorbant molecules in the adsorbate/slab system, and E_{sys} is the total energy of the system. In the case of CRYSTAL calculations, the basis set superposition error (BSSE) was taken into account and the BSSE corrected value is reported.

In order to contain the computational cost, we performed a single Q-E_f trajectory DC SCVIR simulation initialized with the harmonic ZPE velocities, which has been proved to be good enough for calculating the vibrational frequencies of the fundamental transitions in several other systems.[75,86,95] In addition, the angular momentum has been removed to the initial conditions of the trajectory. Thanks to these initial conditions, molecular dynamics involve both the adsorbate and the surface atoms, with the exception of the layers fixed at the bulk position. Harmonic normal modes have been determined through the Density-Functional Perturbation Theory (DFPT)[96] implementation available in Q-E which has been used to compute the Hessian matrix. In the evaluation of the Hessian, we neglect the non-analytic term which corrects the long wavevector limit, i.e. $q \to 0$ limit, of the dynamical matrix for polar crystals, which we verified to have a limited effect on the vibrational frequencies of the adsorbate. Table S2 in the SI shows the convergence of the Hessian and the harmonic vibrational frequency calculations with respect to the k-points sampling for the cases considered below. Born-Oppenheimer molecular dynamics (BOMD) has been performed with an in house adaptation of PlaneWaveSelfConsistentField (PWScf) module

to integrate the equation of motion using the symplectic velocity-Verlet algorithm. For the adsorbed molecules, we perform BOMD in the NVE ensemble for 2500 iterations with a time-step of 10 a.u., thus yielding to 0.6 ps of dynamics. To identify the proper subspace for the DC-SCIVR simulation we proceed as described in Sec. II by averaging over 20 full dimensional Hessian matrices computed within DFPT. Once we identified the subspaces, we compute the projected potential according to Eq. (7) and the Hessians along the trajectory only for the subspace modes of interest, using a finite difference approach starting from the forces obtained by the ab-initio code. These two tasks have been performed through two small codes which determine the necessary atomic configurations according to the algorithms described in the previous section, runs a series of SCF calculations with PWScf, and, after collecting the results, reconstructs the Hessian in the subspace or the projected potential. In particular, for the Hessian evaluation, we first convert the coordinates from Cartesian to normal modes, add a displacement, and then the coordinates are converted back to Cartesian ones. The amplitude of the atomic displacement has been adapted to the surface flatness as $\eta_j = \eta_0/\omega_{H_j}$ with η_0 equal to 5×10^{-4} a.u. with the aim of improving the accuracy in case of flat PES, and to increase the level of accuracy of our SCF cycles we recalculate the forces at the BOMD geometries. The atomic forces obtained from the SCF results are then converted in normal mode coordinates and the matrix elements of the Hessian in the subspace can be computed by a finite difference estimation of the first derivatives, i.e. the forces. This reduces the costs for the evaluation of the Hessian inside the subspace of interest to a number of SCF cycles equal to the dimension of the subspace plus the eventual recalculation of the forces in the equilibrium geometry.

III. RESULTS: VIBRATIONAL SPECTRA FOR ADSORBATES ON TIO_2 ANATASE (101)

Geometry considerations

For all the adsorbates, we choose an adsorption geometry with the molecule adsorbed upon one available Ti_{5c} site with the Carbon or Nitrogen or Oxygen atom pointing toward the surface, because this is the most stable configuration found by previous ab initio calculations (see Ref.s 2, 4, 97, and 98 for the adsorption of CO, Ref.s 99–102 for NO and Ref.s 103–107

Table I. Relevant coordinates and binding energies for CO adsorbed on TiO_2 anatase (101) surface. Comparison of the present results with literature reference values. r(Ti_{5c}–C) is the distance between the Carbon and the Ti_{5c} adsorption site, r(C–O) the intramolecular distance, α(Ti_{5c}-C-O) the angle between these two distances, and BE stands for the classical bottom-of-the-well "Binding Energy".

Method	Layers	Functional	Coverage	r(Ti_{5c}–C) [Å]	r(C–O) [Å]	α(Ti_{5c}-C-O) [°]	BE [eV][a]
CRYSTAL	8L	PBE0	θ=0.5	2.506	1.120	178.65	0.22
Q-E_i	8L	PBE+U	θ=0.25	2.511	1.139	177.86	0.29
Q-E_f	4L	PBE	θ=0.25	2.507	1.139	179.37	0.22
Q-E[b]	6L	PBE+D2	θ=0.125	2.33	1.139		0.262
CRYSTAL09[c]	10L	PBE0	θ=0.25	2.571	1.1202		0.22
VASP[d]		PBE+U	θ=0.33	2.467	1.138		0.34
VASP[e]	6L	PBE	θ=0.5	2.531	1.139	175.74	0.26
CPMD[f]	6L	PBE		2.345	1.129		0.40

[a] Experimental value 0.37 eV[4]
[b] From Ref.4
[c] From Ref.2
[d] From Ref.98
[e] From Ref.97
[f] From Ref.108

for H_2O). Fig. 2 reports the obtained equilibrium geometries for the adsorption of the three molecules, together with the anatase (101) surface atoms. The corresponding CO geometry values of the Figure can be found in Table I. To assess the level of ab initio theory for the dynamics, we have employed different level of theory with different supercell arrangements and DFT functional set-up to be compared with the literature. In the first row of Table I we show our calculations using the CRYSTAL suite of codes with a supercell made of 8 layers, the PBE0 DFT functional and a surface coverage equal to 0.5. The distance between the Carbon end of the molecule and the adsorption surface site Ti_{5c} (r(Ti_{5c}–C)), the intramolecular Carbon-Oxygen distance (r(C–O)) and the angle between them α(Ti_{5c}-C-O) are also reported, together with the binding energy (BE). These values are compared with those obtained using the Q-E arrangements described above. Since Q-E_i proves to be quite computationally intense with 8 Ti layers, we employ it for static calculations only. Instead Q-E_f is a less computationally intense setup, feasible for the classical and semiclassical dynamics calculations. While the binding energy (BE) between the different Q-E set-up differs about 30%, the geometric arrangement changes are less than 1%. The comparison with the literature values show that both our CRYSTAL and Q-E computational set-up, which are reported at the first three row from above in Table I, are accurate. More

Table II. The same as in Table I but for the relevant geometrical coordinates and binding energies for NO adsorbed on the TiO_2 anatase (101) surface.

Method	Layers	Functional	Coverage	r(Ti_{5c}–N) [Å]	r(N–O) [Å]	α(Ti_{5c}-N-O) [°]	BE [eV]
Crystals	8L	PBE0	θ=0.5	2.556	1.131	132.6	0.16
Q-E_i	8L	PBE+U	θ=0.25	2.548	1.159	131.66	0.23
Q-E_f	4L	PBE	θ=0.25	2.435	1.153	131.86	0.27
DMol3[a]	4L	PBE	θ=0.25	2.449	1.144	178.178	0.25
VASP[b]	6L	PBE	θ=0.25	2.512	1.164		0.29

[a] From Ref. 99
[b] From Ref. 100

specifically, our CRYSTAL calculations are consistent with Ref. 2, where the same suite of codes have been employed, and our Q-E calculations are reproducing other plane-wave ones, compatible with the different slab and coverage arrangements.

In Table II, we report the results of the same calculations but for the NO adsorption. In this case, the comparison with the literature results is poor. Specifically, the α(Ti_{5c}-N-O) angle differs considerably. The following vibrational analysis shows that our geometry is indeed a minimum and we could not find a minimum at the angle suggested in the literature. For these reasons, we perform our classical and semiclassical calculations starting from our minimum geometry. Also, we have a slight different value for the r(Ti_{5c}–N) distance between the two Q-E set-up. However, we consider this difference quite contained and hence the Q-E_f arrangement good enough for our dynamics calculations.

Finally we look at a suitable computational set-up to describe the molecular water adsorption on the TiO_2 anatase (101) surface. In Tab. III, our well tested Q-E_f method results are quite in agreement with the literature values both for geometry and energetics and a Q-E_i calculation was not necessary, given the presence in the literature of several other Q-E calculations, some of them reported in Table III. Specifically, the distances and the angle are quite similar for all type of theoretical approaches, while the BE may differ, depending on the code employed. Our results are consistent with the literature Q-E ones. Thus, we adopt the Q-E_f for classical and quantum dynamics calculations.

Table III. The same as in Table I but for the relevant geometrical coordinates and binding energies for H_2O adsorbed on the TiO_2 anatase (101) surface.

				r(Ti_{5c}–O) [Å]	r(O–H) [Å]	d(O_{2c}-H) [Å]	α(H-O-H) [°]	BE [eV][a]
Q-E_f	4L	PBE	θ=0.25	2.283	0.984	2.284	103.89	0.76
CASTEP[b]	8L	PBE		2.236	0.995	2.101	102.585	0.948
CASTEP[c]	4L	PBE		2.245	0.993	2.122		0.916
Q-E[d]		PBE	θ=0.17	2.30		2.26		0.71
Q-E[e]		PBE	θ=0.17	2.300		2.257/2.263		0.720
Crystal14[f]	4L	PBE	θ=0.25			2.25		0.71
Crystal14[f]	4L	HSE06	θ=0.25			2.29		0.84

[a] Experimental value 0.5-0.7 eV.[109]
[b] From Ref.104
[c] From Ref.103
[d] From Ref.106
[e] From Ref.105
[f] From Ref.107

Frequencies calculations

The vibrational frequency calculations are done at three different levels of theory. First, at the harmonic level by diagonalization of the Hessian matrix at the minimum adsorption geometry. Second, to include anharmonic effects, we run BO classical dynamics, where the trajectory energy is equal to the harmonic Zero Point vibrational Energy (ZPE) value and to obtain the set of frequencies employing Eq. (8). This is a classical calculation which reproduces the fundamental vibrational frequencies, including classical resonances between modes but without any quantum mechanical effect. We label this level of calculations as "quasi-classical", as explained at the end of sub-Section II. Third, we employ our DC SCIVR approach to calculate the full quantum mechanical power spectrum, which includes the actual anharmonic ZPE value, the quantum fundamentals frequencies and the overtones and combination bands. Also, eventual quantum resonances or tunneling effects due to the delocalization of the lighter nuclei (such as Hydrogen) can be reproduced, as it has been shown in previous calculations using the same method.[13,70,81,86,95] As described above, the DC SCIVR approach needs a suitable choice of the reduced dimensionality subspace which properly describes the vibrational motion of the adsorbate. The most drastic choice would be to consider the internal vibrational modes of the adsorbate as the modes composing the subspace. This approximation is actually contemplated in our method in Eq.(9) for values

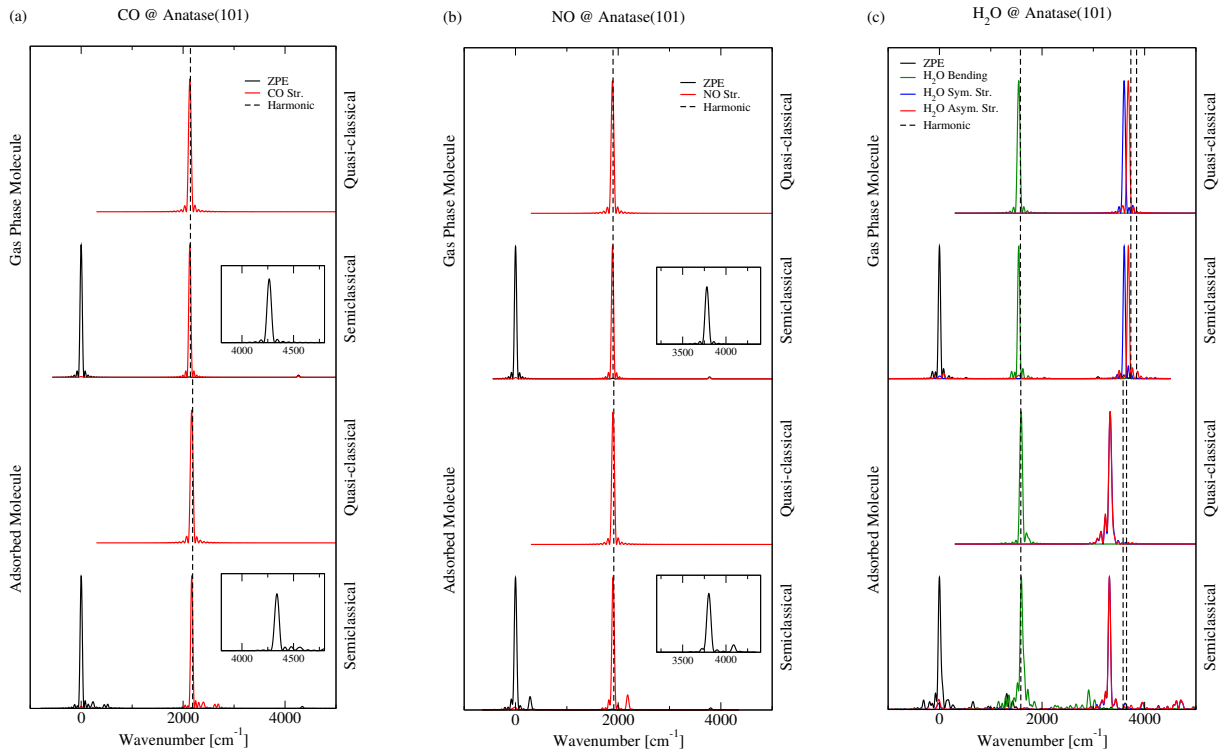

Figure 3. Harmonic, quasi-classical and semiclassical (DC-SCIVR) spectra for CO (left, panel(a)), NO (center, panel(b)) and H_2O (right, panel(c)) in gas phase and adsorbed on the TiO_2 anatase (101) surface. The semiclassical spectra have been shifted to have the ZPE peak at zero frequency for better comparison with the quasi-classical and harmonic results. The insets highlight the semiclassical overtones. H_2O angular momentum was removed by initializing the classical trajectory as it would be a system isolated from the surface.

of ϵ large enough and it brings a monodimensional space for the CO and NO adsorption and a 3-dimensional one for H_2O. Since in all these three cases the spectrum resulting from such a choice is quite noisy, we proceed by enlarging the subspace and including other surface and bulk modes by gradually reducing the value of ϵ. Following the procedure described in Section II and in Eq.(9), we generate all the spectra reported in the SI (Fig. S1) and the final vibrational adsorbate subspace dimensionality is 3 for CO, 4 for NO and 14 for H_2O.

Fig. 3 and the corresponding Table IV report the results by applying the three levels of theory (harmonic, quasi-classical and semiclassical) to the calculation of the fundamental vibrational spectra for the three adsorbates, both in gas phase (before adsorption) and after adsorption, using QE for both phases. In the left part of Fig. 3 (panel (a)) and the values in the CO column of Tab. IV, one can see the spectra for the CO molecule, both in gas phase or after adsorption.The agreement of the harmonic results with the experimental values is very

Table IV. Comparison of fundamental vibrational frequencies for the stretching modes of CO and NO and stretching and bending modes of H_2O in gas phase and after adsorption on the TiO_2 anatase (101) surface. We employ the QE code both for gas and adsorbed phases calculations for a better comparison. All the frequencies are in cm^{-1}.

	CO	NO	H_2O		
Gas Phase					
Experiment[a]	2143	1876	1595	3657	3756
Harmonic	2144	1900	1580	3731	3843
Quasi-classical	2132	1890	1545	3600	3681
DC SCIVR	2134	1890	1547	3603	3683
Surface Adsorbed					
Experiment	2180[b], 2185[c]	1901[d]	1615[e] ,1635[f]	from 3300 to 3700[f]	from 3300 to 3700[f]
Harmonic	2187	1914	1586	3580	3647
Quasi-classical	2169	1901	1592	3328	3327
DC SCIVR	2168	1901	1596	3314	3312

[a] From Ref. 110
[b] From Ref. 111
[c] From Ref. 4
[d] From Ref. 102
[e] From Ref. 112
[f] From Refs.113 and 114

good. In fact, several theoretical calculations of vibrational frequencies at harmonic level have been successfully compared to experiments for the adsorbed CO molecule.[2,4,98] Quasi-classical and semiclassical simulations find fundamental frequency values lower by an equal amount of almost $20\,cm^{-1}$.The DC-SCIVR plots in panel (a) of Fig. 3 show a small intensity peak in correspondence of the CO internal vibrational overtone, which is highlighted by the inset, around 4300 cm^{-1}, both in gas and condensed phase. In addition, the DC-SCIVR spectrum for the adsorbate shows some small intensity peaks on the right side of the ZPE one. These peaks correspond to even overtone excitations (since $\boldsymbol{\gamma} = 1$) and are due to the coupling between the molecule and the surface. These overtones are mainly originated by the two additional modes included in the subspace, which are frustrated rotations of the CO with axis respectively along the $[\bar{1}01]$ direction at 255 cm^{-1} and along the [010] direction at 230 cm^{-1} reported in Fig.S2. In the same panel and from Tab. IV, we observe about $40\,cm^{-1}$ blue-shift in going from gas to adsorbed phase. This is a well known shift and it is often explained in terms of electronic back donation from the bulk to the LUMO (Lowest Unoccupied Molecular Orbital) of the adsorbate, which results in a stronger CO

bond strength. Another possible explanation is given by the Pauli repulsion between the CO electronic cloud and the surface electronic cloud.[108] A third possible explanation is given by the Stark effect that the surface electrostatic field may induce in the Carbon cation.[37,108,115]

We now turn our attention to the vibrational description of the NO adsorption reported in panel (b) of Fig. 3 and in the third column of Table IV. Given the similarity between the CO and NO, analogous considerations can be applied. However, in this case both in the gas and condensed phase, a better agreement with experimental results is reached only after inclusion of anharmonic effects, i.e. using the BOMD dynamics simulations. Here, the harmonic frequency is about $10\,\mathrm{cm}^{-1}$ in the gas phase and $15\,\mathrm{cm}^{-1}$ in condensed phase larger than the quasi-classical and semiclassical ones, which are about the same values. The similarity between quasi-classical and semiclassical is expected, since NO and TiO_2 are heavy nuclei compounds. The only spectroscopic difference between the two approaches consists in the presence of overtones that the semiclassical method can detect. Overtone peaks are visible in the adsorbate spectrum, both at the right side of the ZPE and of the fundamental NO vibrational peak, which are highlighted in the Fig.(3) insets. These peaks are given by the surface and bulk modes that are mostly coupled to the NO internal stretch and belonging to the four dimensional DC-SCIVR vibrational subspace, as shown in Fig.S2. Despite the fact that nitric oxide is a molecular probe similar to CO, the interaction with non transition metal centers or with empty d orbital transition metals can be weaker because NO, being a radical, has a tendency to dimerize.[37] The interaction comes through an extra electron at HOMO (Highest Occupied Molecular Orbital). For these reason, the blueshift is very much contained in this case.

The adsorption of H_2O is an example of a more complex spectroscopic structure, composed of adsorbant-surface couplings and relevant overtones and combination bands.[105,116–118] Here, both in gas and condensed phase, the simple harmonic approach is not accurate for the description of the fundamental frequency estimates, as shown in Tab. IV and Fig. 3. The effect of the anharmonicity corresponds to about a $150\,\mathrm{cm}^{-1}$ lower frequency shift in the gas phase and a $200\,\mathrm{cm}^{-1}$ shift for the adsorbate. Also in this case, the quasi-classical and semiclassical simulations provide the same answer for the fundamental frequency values showing an almost degeneracy for the symmetric and asymmetric stretches after adsorption. Despite this agreement in terms of fundamental frequencies, by looking at the vibrational spectrum of the adsorbate, we can appreciate the fact that in the semiclassical spectrum we

obtain a variety of signals that reproduces all the overtones and combination bands present in such a complex system and that the quasi-classical simulation can not reproduce. The intensity of these peaks is lower than the fundamental ones because they are located farther in energy from the classical trajectories and the Gaussian wavepacket energy shell. Also, the intensities of the overtones peaks are reduced because H_2O trajectory initial conditions. However, a bending overtone is clearly visible towards 2900 cm^{-1} and combination bands due to the coupling with the surface are present at around 4600-4700 cm^{-1}. Finally, we note that the bending blue shift, observed from both theory and experiment in going from the gas phase to the condensed one, may be due to the fact that there is less room for the molecule to bend in condensed phase and the vibrational frequency is consequently stiffer. Once again, the harmonic approximation is missing to reproduce this effect as well.

As we have mentioned above, we have removed the angular momentum from trajectories initial conditions in previous simulations. In the case of the H_2O adsorbate, we added an additional constraint. The angular momentum was removed for the H_2O coordinates separately, as it would be a system isolated from the surface. This is necessary to avoid that, after about a thousand steps, the molecule starts rotating with respect to the surface. If this constrain is relaxed and the molecule is free to reorient during the dynamics, we obtain the spectra reported in Fig.(4). The comparison between these spectra and those on the bottom part of Fig.(3)c shows that the H_2O rotation splits the fundamental peaks. In addition to the splitting of the two almost degenerate symmetric and asymmetric stretch modes, the semiclassical simulation is able to provide several additional overtone peaks originated by the coupling between the molecular stretching, the frustated rotations and the surface modes. Even if the signal to noise ratio in this case is slightly worse than in Fig.(3)c, because of the introduction of the floppiest modes in the spectrum, some overtones and combination bands can be identified. Eventually, Fig.(4) shows how the hindered internal rotations of the water molecule with respect to the surface generates several overtone spectroscopic features. This is still quite different from the experimental spectrum[113,114] where a large band is observed in correspondence of the OH stretching frequency. In fact, our divide-and-conquer approach allows us to filter out the signal originated from most of the phonon bath and the differences with the experimental spectrum is also due to this filtering.

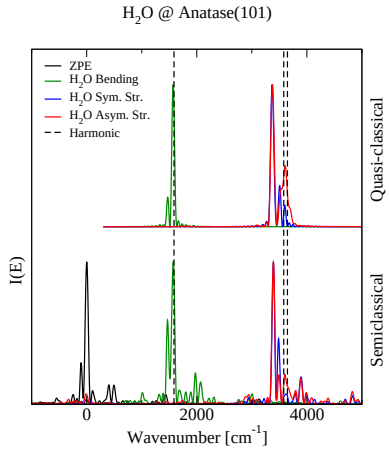

Figure 4. Vibrational frequencies of H_2O on the TiO_2 anatase (101) surface without the angular momentum removal from the trajectory initial conditions. All the frequencies are in cm^{-1}. The semiclassical spectra have been shifted to have the ZPE peak at zero frequency for better comparison with the quasi-classical and harmonic results.

Adsorbate-surface interactions

We now investigate the adsorbate-surface couplings by looking at the surface atom displacements for each mode. The eigen-displacements corresponding to the aforementioned adsorbant subspace modes are represented in Fig. 5 as a colormap of the moduli of its components on each atom. In each panel the adsorbate atoms are indicated by their corresponding atomic label. The colormap is such that more intense colored atoms correspond to those ones more involved in the motion of the surface modes coupled with the adsorbate.

Fig. 5 shows that frustated rotational molecular modes are those more coupled to the internal molecular modes for all three kind of adsorption. These modes are quite delocalized over the surface. However, the frustated modes involve the surface atoms in quite a different pattern, according to the type of adsorbed molecule. In the case of CO adsorption (see panel (a) of Fig.5) the surface oxygen and titanium atoms are equally involved in the surface modes coupled with the adsorbant. In the case of the NO adsorption (panel (b) of Fig. 5) similar considerations are valid with the addition that the coupling between the adsorbate and the surface atoms is definitely greater.

Finally, in the case of water adsorption (panel (c) of Fig. 5) the main coupling is again with the frustated rotational modes. However, in this case, the Oxygen atoms are mainly coupled to the adsorbate. We think that this selective coupling is due to the fact that the frustated rotational motion involves mainly the adsorbate Hydrogen atoms, which naturally

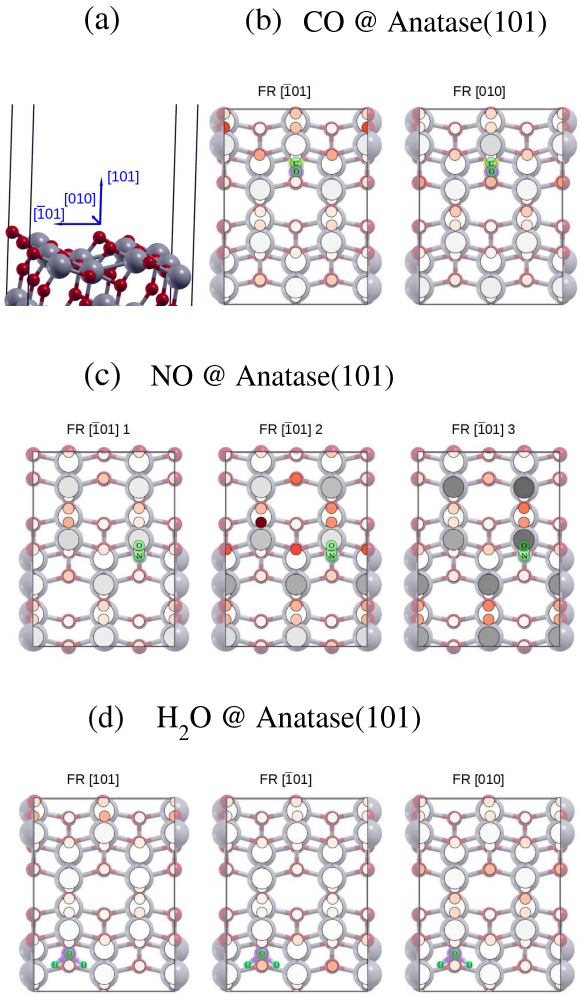

Figure 5. Axes of rotation in panel (a) and color map representation of the titania normal modes for the CO in panel (b), NO in panel (c), and H_2O in panel (d) adsorbed on the TiO_2 anatase (101) surface. The bigger is the atomic mass-scaled displacement, the more intense is the atom color. Acronym "FR" stands for Frustated Rotations and it is followed by the label of the related rotational axis. The modes are those belonging to the CO and NO DC-SCIVR subspaces, which are respectively 3 and 4 dimensional. In the case of H_2O, a representative number of titania modes belonging to the 14-dimensional subspace are chosen.

polarize and couple more with the Oxygen electronic cloud.

IV. CONCLUSIONS

In the present work we applied for the first time a divide-and-conquer semiclassical strategy (DC SCIVR) to calculate the vibrational frequencies of molecules adsorbed on surfaces.

A homemade code that interface with the Q-E suite of codes have been generated and three representative molecular adsorption processes have been chosen, i.e. CO, NO and H_2O on anatase TiO_2 (101) surface. DC SCIVR is based on full dimensional classical trajectories and it properly accounts for all kind of couplings between the adsorbate and the slab. The comparison with experimental results shows that the harmonic approximation is enough to describe the adsorption of CO, while it is necessary to include at least classical anharmonic effects for a correct calculation of the NO frequencies. In these cases and if one is interested only on the fundamental internal adsorbate frequency, classical dynamics is a valuable tool and cheaper than the semiclassical simulation, which requests the projected potential and the Hessian calculations. Instead, an approach able to reproduce quantum nuclear effects should be preferred for a more realistic description of a system like the H_2O absorbed on anatase TiO_2 (101) surface, given the presence of several overtones and combination bands with the phonon bath. This was somehow expected, given the light hydrogen atoms.

As far as the accuracy is concerned, in same cases, as the internal stretch of the CO molecule and the gas-phase bending of the water molecule, the anharmonic results are less accurate than the harmonic ones, if compared with the experimental values. Since this is equally true for the quasi-classical and the semiclassical estimates, we impute this discrepancy to the level of ab initio theory. In particular, in the case of water gas-phase bending, the planewave setup is not the most suitable one and we have chosen it only for having a direct comparison with the condensed phase values. Finally, plots of the eigen-displacements of the titania modes most coupled to the adsorbate are reported. These show how the coupling between the adsorbate and the surface is not local and it does involve several atoms.

These considerations will possible open the route for a new spectroscopic view and an alternative way to rationalize catalytic processes for better functional material engineering.

SUPPLEMENTARY MATERIAL

See supplementary material for bulk lattice parameters, k-points convergence of vibrational frequencies, the choice of each adsorbate vibrational space, and additional semiclassical spectra.

ACKNOWLEDGMENTS

The authors thank Dr. R. Conte, Dr. D. Ceresoli and Dr. L. Mino for useful discussions. We acknowledge financial support from the European Research Council (ERC) under the European Union's Horizon 2020 research and innovation programme (Grant Agreement No. [647107]-SEMICOMPLEX ERC-2014-CoG) and from the Italian Ministery of Education, University, and Research (MIUR) (FARE programme R16KN7XBRB-project QURE). We acknowledge the CINECA award under the ISCRA initiative, for the availability of high performance computing resources and support (Grants Nr. HP10CV2CBQ and Nr. HP10CGH9YR).

REFERENCES

[1]L. Mino, A. Zecchina, G. Martra, A. M. Rossi, and G. Spoto, Appl. Catal. B-Environ. **196**, 135 (2016).

[2]L. Mino, A. M. Ferrari, V. Lacivita, G. Spoto, S. Bordiga, and A. Zecchina, J. Phys. Chem. C **115**, 7694 (2011).

[3]L. Mino, G. Spoto, S. Bordiga, and A. Zecchina, J. Phys. Chem. C **116**, 17008 (2012).

[4]M. Setvin, M. Buchholz, W. Hou, C. Zhang, B. Stöger, J. Hulva, T. Simschitz, X. Shi, J. Pavelec, G. S. Parkinson, M. Xu, Y. Wang, M. Schmid, C. Wöll, A. Selloni, and U. Diebold, J. Phys. Chem. C **119**, 21044 (2015).

[5]P. G. Lustemberg and D. A. Scherlis, J. Chem. Phys. **138**, 124702 (2013).

[6]G. Tabacchi, M. Fabbiani, L. Mino, G. Martra, and E. Fois, Angew. Chem. Int. Ed. **58**, 12431 (2019).

[7]D. R. Galimberti, A. Milani, M. Tommasini, C. Castiglioni, and M.-P. Gaigeot, J. Chem. Theory Comput. **13**, 3802 (2017).

[8]A. Witt, S. D. Ivanov, M. Shiga, H. Forbert, and D. Marx, J. Chem. Phys. **130**, 194510 (2009).

[9]M. Tommasini, G. Longhi, S. Abbate, and G. Zerbi, J. Raman Spectrosc. **45**, 89 (2014).

[10]D. M. Benoit, J. Phys. Chem. A **119**, 11583 (2015).

[11]M. Ceotto, G. Di Liberto, and R. Conte, Phys. Rev. Lett. **119**, 010401 (2017).

[12]G. Di Liberto, R. Conte, and M. Ceotto, J. Chem. Phys. **148**, 014307 (2018).

[13]G. Di Liberto, R. Conte, and M. Ceotto, J. Chem. Phys. **148**, 104302 (2018).

[14]C. Zhang and A. Michaelides, Surf. Sci. **605**, 689 (2011).

[15]L. J. Lauhon and W. Ho, Phys. Rev. Lett. **85**, 4566 (2000).

[16]E. M. McIntosh, K. T. Wikfeldt, J. Ellis, A. Michaelides, and W. Allison, J. Phys. Chem. Lett. **4**, 1565 (2013).

[17]G. Kyriakou, E. R. M. Davidson, G. Peng, L. T. Roling, S. Singh, M. B. Boucher, M. D. Marcinkowski, M. Mavrikakis, A. Michaelides, and E. C. H. Sykes, ACS Nano **8**, 4827 (2014).

[18]T. Kumagai, M. Kaizu, H. Okuyama, S. Hatta, T. Aruga, I. Hamada, and Y. Morikawa, Phys. Rev. B **79**, 035423 (2009).

[19]T. Mitsui, M. K. Rose, E. Fomin, D. F. Ogletree, and M. Salmeron, Science **297**, 1850 (2002).

[20]V. A. Ranea, A. Michaelides, R. Ramírez, P. L. de Andres, J. A. Vergés, and D. A. King, Phys. Rev. Lett. **92**, 136104 (2004).

[21]T. Kumagai, M. Kaizu, S. Hatta, H. Okuyama, T. Aruga, I. Hamada, and Y. Morikawa, Phys. Rev. Lett. **100**, 166101 (2008).

[22]T. Koitaya and J. Yoshinobu, Chem. Rec. **14**, 848 (2014).

[23]X. Meng, J. Guo, J. Peng, J. Chen, Z. Wang, J.-R. Shi, X.-Z. Li, E.-G. Wang, and Y. Jiang, Nat. Phys. **11**, 235 (2015).

[24]Y. Litman, D. Donadio, M. Ceriotti, and M. Rossi, J. Chem. Phys. **148**, 102320 (2018).

[25]H. Chen, C. E. Nanayakkara, and V. H. Grassian, Chem. Rev. **112**, 5919 (2012).

[26]A. Kudo and Y. Miseki, Chem. Soc. Rev. **38**, 253 (2009).

[27]F. E. Osterloh, Chem. Soc. Rev. **42**, 2294 (2013).

[28]C. Luo, X. Ren, Z. Dai, Y. Zhang, X. Qi, and C. Pan, ACS Appl. Mater. Inter. **9**, 23265 (2017).

[29]Q. Guo, C. Zhou, Z. Ma, Z. Ren, H. Fan, and X. Yang, Chem. Soc. Rev. **45**, 701 (2016).

[30]U. Diebold, Surf. Sci. Rep. **48**, 53 (2003).

[31]M. A. Henderson, Surf. Sci. Rep. **66**, 185 (2011).

[32]A. Selloni, "Titania and its outstanding properties: Insights from first principles calculations," in *Handbook of Materials Modeling: Applications: Current and Emerging Materials*, edited by W. Andreoni and S. Yip (Springer International Publishing, 2018) pp. 1–23.

[33]I. Alessandri, J. Am. Chem. Soc. **135**, 5541 (2013).

[34]N. Serpone and A. V. Emeline, J. Phys. Chem. Lett. **3**, 673 (2012).

[35]J. Oviedo, R. Sánchez-de Armas, M. A. San Miguel, and J. F. Sanz, J. Phys. Chem. C **112**, 17737 (2008).

[36]Y. Wang and C. Wöll, Chem. Soc. Rev. **46**, 1875 (2017).

[37]C. Lamberti, A. Zecchina, E. Groppo, and S. Bordiga, Chem. Soc. Rev. **39**, 4951 (2010).

[38]A. Mahdavi-Shakib, J. M. Arce-Ramos, R. N. Austin, T. J. Schwartz, L. C. Grabow, and B. G. Frederick, J. Phys. Chem. C **123**, 24533 (2019).

[39]R. Conte and M. Ceotto, *Semiclassical Molecular Dynamics for Spectroscopic Calculations* (Wiley, book chapter, accepted).

[40]E. J. Heller, Acc. Chem. Res. **14**, 368 (1981).

[41]R. P. Feynman and A. R. Hibbs, *Quantum mechanics and path integrals* (McGraw-Hill, 1965).

[42]W. H. Miller, J. Phys. Chem. A **105**, 2942 (2001).

[43]H. Kreek and R. A. Marcus, J. Chem. Phys. **61**, 3308 (1974).

[44]M. C. Gutzwiller, J. Math. Phys. **8**, 1979 (1967).

[45]W. H. Miller, J. Chem. Phys. **53**, 3578 (1970).

[46]J. H. Van Vleck, Proc. Natl. Acad. Sci. **14**, 178 (1928).

[47]W. H. Miller, Proc. Natl. Acad. Sci. USA **102**, 6660 (2005).

[48]W. H. Miller, J. Chem. Phys. **53**, 1949 (1970).

[49]E. J. Heller, J. Chem. Phys. **75**, 2923 (1981).

[50]K. G. Kay, J. Chem. Phys. **101**, 2250 (1994).

[51]K. G. Kay, J. Chem. Phys. **100**, 4432 (1994).

[52]E. Pollak and E. Martin-Fierro, J. Chem. Phys. **126**, 164107 (2007).

[53]E. Pollak, "The Semiclassical Initial Value Series Representation of the Quantum Propagator," in *Quantum Dynamics of Complex Molecular Systems* (Springer Berlin Heidelberg, Berlin, Heidelberg, 2007) pp. 259–271.

[54]S. Bonella, D. Montemayor, and D. F. Coker, Proc. Natl. Acad. Sci. **102**, 6715 (2005).

[55]D. V. Shalashilin and M. S. Child, J. Chem. Phys. **115**, 5367 (2001).

[56]X. Ma, G. Di Liberto, R. Conte, W. L. Hase, and M. Ceotto, J. Chem. Phys. **149**, 164113 (2018).

[57]M. Buchholz, E. Fallacara, F. Gottwald, M. Ceotto, F. Grossmann, and S. D. Ivanov, Chem. Phys. **515**, 231 (2018).

[58]M. S. Church, S. V. Antipov, and N. Ananth, J. Chem. Phys. **146**, 234104 (2017).

[59]S. V. Antipov, Z. Ye, and N. Ananth, J. Chem. Phys. **142**, 184102 (2015).

[60]T. Begusic, J. Roulet, and J. Vanicek, J. Chem. Phys. **149**, 244115 (2018).

[61]J. Liu, Int. J. Quantum Chem. **115**, 657 (2015).

[62]A. L. Kaledin and W. H. Miller, J. Chem. Phys. **118**, 7174 (2003).

[63]A. L. Kaledin and W. H. Miller, J. Chem. Phys. **119**, 3078 (2003).

[64]Y. Elran and K. Kay, J. Chem. Phys. **110**, 8912 (1999).

[65]M. Ceotto, S. Atahan, S. Shim, G. F. Tantardini, and A. Aspuru-Guzik, Phys. Chem. Chem. Phys. **11**, 3861 (2009).

[66]M. Ceotto, S. Atahan, G. F. Tantardini, and A. Aspuru-Guzik, J. Chem. Phys. **130**, 234113 (2009).

[67]M. Ceotto, D. Dell'Angelo, and G. F. Tantardini, J. Chem. Phys. **133**, 054701 (2010).

[68]M. Ceotto, G. F. Tantardini, and A. Aspuru-Guzik, J. Chem. Phys. **135**, 214108 (2011).

[69]M. Ceotto, S. Valleau, G. F. Tantardini, and A. Aspuru-Guzik, J. Chem. Phys. **134**, 234103 (2011).

[70]R. Conte, A. Aspuru-Guzik, and M. Ceotto, J. Phys. Chem. Lett. **4**, 3407 (2013).

[71]E. J. Heller, J. Chem. Phys. **94**, 2723 (1991).

[72]M. F. Herman and E. Kluk, Chem. Phys. **91**, 27 (1984).

[73]E. Kluk, M. F. Herman, and H. L. Davis, J. Chem. Phys. **84**, 326 (1986).

[74]M. L. Brewer, J. S. Hulme, and D. E. Manolopoulos, J. Chem. Phys. **106**, 4832 (1997).

[75]R. Conte, F. Gabas, G. Botti, Y. Zhuang, and M. Ceotto, J. Chem. Phys. **150**, 244118 (2019).

[76]M. Ceotto, Y. Zhuang, and W. L. Hase, J. Chem. Phys. **138**, 054116 (2013).

[77]Y. Zhuang, M. R. Siebert, W. L. Hase, K. G. Kay, and M. Ceotto, J. Chem. Theory Comput. **9**, 54 (2013).

[78]R. Conte, L. Parma, C. Aieta, A. Rognoni, and M. Ceotto, J. Chem. Phys. **151**, 214107 (2019).

[79]T. Begusic, M. Cordova, and J. Vanicek, J. Chem. Phys. **150**, 154117 (2019).

[80]G. Di Liberto and M. Ceotto, J. Chem. Phys. **145**, 144107 (2016).

[81]F. Gabas, R. Conte, and M. Ceotto, J. Chem. Theory Comput. **13**, 2378 (2017).

[82]D. Tamascelli, F. S. Dambrosio, R. Conte, and M. Ceotto, J. Chem. Phys. **140**, 174109 (2014).

[83]M. Buchholz, F. Grossmann, and M. Ceotto, J. Chem. Phys. **144**, 094102 (2016).

[84]M. Buchholz, F. Grossmann, and M. Ceotto, J. Chem. Phys. **147**, 164110 (2017).

[85]M. Buchholz, F. Grossmann, and M. Ceotto, J. Chem. Phys. **148**, 114107 (2018).

[86]F. Gabas, G. Di Liberto, and M. Ceotto, J. Chem. Phys. **150**, 224107 (2019).

[87]G. Bertaina, G. Di Liberto, and M. Ceotto, J. Chem. Phys. **151**, 114307 (2019).

[88]M. Micciarelli, R. Conte, J. Suarez, and M. Ceotto, J. Chem. Phys. **149**, 064115 (2018).

[89]M. Micciarelli, F. Gabas, R. Conte, and M. Ceotto, J. Chem. Phys. **150**, 184113 (2019).

[90]M. Valiev, E. Bylaska, N. Govind, K. Kowalski, T. Straatsma, H. V. Dam, D. Wang, J. Nieplocha, E. Apra, T. Windus, and W. de Jong, Comput. Phys. Commun. **181**, 1477 (2010).

[91]P. Giannozzi, S. Baroni, N. Bonini, M. Calandra, R. Car, C. Cavazzoni, D. Ceresoli, G. L. Chiarotti, M. Cococcioni, I. Dabo, A. D. Corso, S. de Gironcoli, S. Fabris, G. Fratesi, R. Gebauer, U. Gerstmann, C. Gougoussis, A. Kokalj, M. Lazzeri, L. Martin-Samos, N. Marzari, F. Mauri, R. Mazzarello, S. Paolini, A. Pasquarello, L. Paulatto, C. Sbraccia, S. Scandolo, G. Sclauzero, A. P. Seitsonen, A. Smogunov, P. Umari, and R. M. Wentzcovitch, J. Phys.-Conddens. Mat. **21**, 395502 (2009).

[92]P. Giannozzi, O. Andreussi, T. Brumme, O. Bunau, M. B. Nardelli, M. Calandra, R. Car, C. Cavazzoni, D. Ceresoli, M. Cococcioni, N. Colonna, I. Carnimeo, A. D. Corso, S. de Gironcoli, P. Delugas, R. A. DiStasio, A. Ferretti, A. Floris, G. Fratesi, G. Fugallo, R. Gebauer, U. Gerstmann, F. Giustino, T. Gorni, J. Jia, M. Kawamura, H.-Y. Ko, A. Kokalj, E. Küçükbenli, M. Lazzeri, M. Marsili, N. Marzari, F. Mauri, N. L. Nguyen, H.-V. Nguyen, A. O. de-la Roza, L. Paulatto, S. Poncé, D. Rocca, R. Sabatini, B. Santra, M. Schlipf, A. P. Seitsonen, A. Smogunov, I. Timrov, T. Thonhauser, P. Umari, N. Vast, X. Wu, and S. Baroni, J. Phys.-Conddens. Mat. **29**, 465901 (2017).

[93]R. Dovesi, R. Orlando, A. Erba, C. M. Zicovich-Wilson, B. Civalleri, S. Casassa, L. Maschio, M. Ferrabone, M. De La Pierre, P. D'Arco, Y. Noël, M. Causà, M. Rérat, and B. Kirtman, Int. J. Quantum Chem. **114**, 1287 (2014).

[94]R. Dovesi, V. R. Saunders, C. Roetti, R. Orlando, C. M. Zicovich-Wilson, F. Pascale, B. Civalleri, K. Doll, N. M. Harrison, I. J. Bush, P. D'Arco, M. Llunell, M. Causà, and Y. Noël, *CRYSTAL14 User's Manual*, University of Torino, Torino (2014).

[95]F. Gabas, G. Di Liberto, R. Conte, and M. Ceotto, Chem. Sci. **9**, 7894 (2018).

[96]S. Baroni, S. de Gironcoli, A. Dal Corso, and P. Giannozzi, Rev. Mod. Phys. **73**, 515 (2001).

[97]R. Wanbayor, P. Deák, T. Frauenheim, and V. Ruangpornvisuti, J. Chem. Phys. **134**, 104701 (2011).

[98]H.-Y. T. Chen, S. Tosoni, and G. Pacchioni, Surf. Sci. **652**, 163 (2016).

[99]W. Zhao, F. H. Tian, X. Wang, L. Zhao, Y. Wang, A. Fu, S. Yuan, T. Chu, L. Xia, J. C. Yu, and Y. Duan, J. Colloid Interf. Sci. **430**, 18 (2014).

[100]L. Huang, K. Zha, S. Namuangruk, A. Junkaew, X. Zhao, H. Li, L. Shi, and D. Zhang, Catal. Sci. Technol. **6**, 8516 (2016).

[101]Q. Liu, L. Liu, and W. Xiao, ChemPhysChem **18**, 653 (2017).

[102]L. Mino, F. Moriggi, M. Cazzaniga, G. Spoto, G. Martra, and M. Ceotto, in preparation.

[103]Z. Zhao, Z. Li, and Z. Zou, Phys. Lett. A **375**, 2939 (2011).

[104]Z. Zhao, Z. Li, and Z. Zou, J. Phys. Chem. C **116**, 7430 (2012).

[105]U. Aschauer, Y. He, H. Cheng, S.-C. Li, U. Diebold, and A. Selloni, J. Phys. Chem. C **114**, 1278 (2010).

[106]U. J. Aschauer, A. Tilocca, and A. Selloni, Int. J. Quantum Chem. **115**, 1250 (2015).

[107]R. Martinez-Casado, G. Mallia, N. M. Harrison, and R. Pérez, J. Phys. Chem. C **122**, 20736 (2018).

[108]C. Deiana, E. Fois, G. Martra, S. Narbey, F. Pellegrino, and G. Tabacchi, ChemPhysChem **17**, 1956 (2016).

[109]M. Egashira, S. Kawasumi, S. Kagawa, and T. Seiyama, B. Chem. Soc. Jpn. **51**, 3144 (1978).

[110]"Nist computational chemistry comparison and benchmark database, nist standard reference database number 101, release 19, april 2018, editor: Russell d. johnson iii, http://cccbdb.nist.gov/,".

[111]M. Xu, Y. Gao, E. M. Moreno, M. Kunst, M. Muhler, Y. Wang, H. Idriss, and C. Wöll, Phys. Rev. Lett. **106**, 138302 (2011).

[112]H. Zhang, P. Zhou, Z. Chen, W. Song, H. Ji, W. Ma, C. Chen, and J. Zhao, J. Phys. Chem. C **121**, 2251 (2017).

[113]H. Sheng, H. Zhang, W. Song, H. Ji, W. Ma, C. Chen, and J. Zhao, Angew. Chem. Int. Ed. **54**, 5905 (2015).

[114]L. Mino, F. Pellegrino, S. Rades, J. Radnik, V.-D. Hodoroaba, G. Spoto, V. Maurino, and G. Martra, ACS Appl. Nano Mater. **1**, 5355 (2018).

[115]G. Pacchioni, A. M. Ferrari, and P. S. Bagus, Surf. Sci. **350**, 159 (1996).

[116]C. Sun, L.-M. Liu, A. Selloni, G. Q. M. Lu, and S. C. Smith, J. Mater. Chem. **20**, 10319 (2010).

[117]A. Vittadini, A. Selloni, F. Rotzinger, and M. Grätzel, Phys. Rev. Lett. **81**, 2954 (1998).

[118]M. F. Calegari Andrade, H.-Y. Ko, R. Car, and A. Selloni, J. Phys. Chem. Lett. **9**, 6716 (2018).

Glycine

(a)
2 Modes
ZPE
NH Sym. Str.
NH Asym. Str.
(b)
5 Modes (20 Hessians)
ε = 7 x 10^-6
(c)
7 Modes (20 Hessians)
ε = 4 x 10^-6
(d)
16 Modes (20 Hessians)
ε = 2 x 10^-6
(e)
16 Modes (2500 Hessians)
ε = 2 x 10^-6
(f)
Full dimensional
0
2000
4000
Wavenumber [cm^-1]

(a) CO @ Anatase(101)

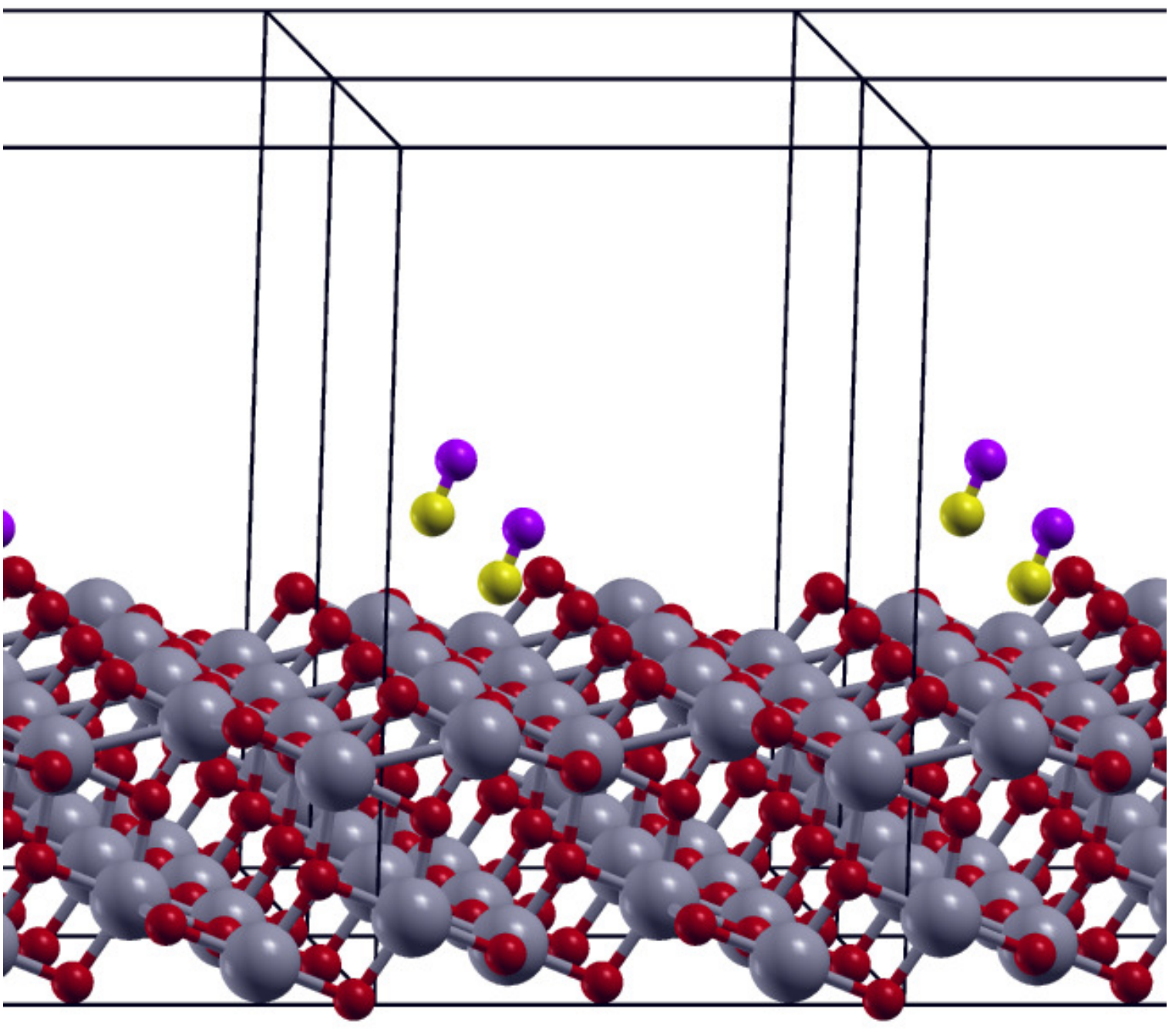

(b) NO @ Anatase(101)

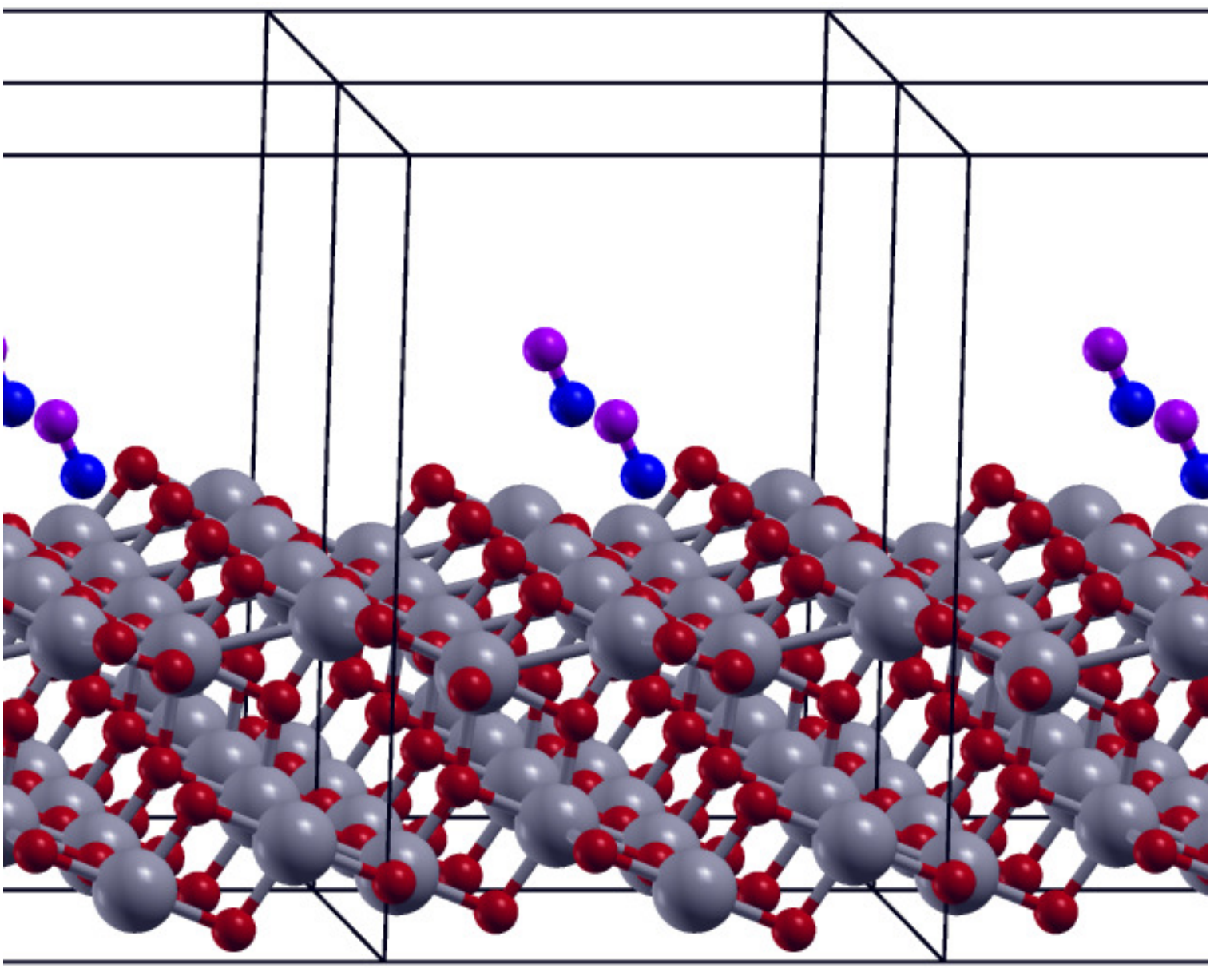

(c) H_2O @ Anatase(101)

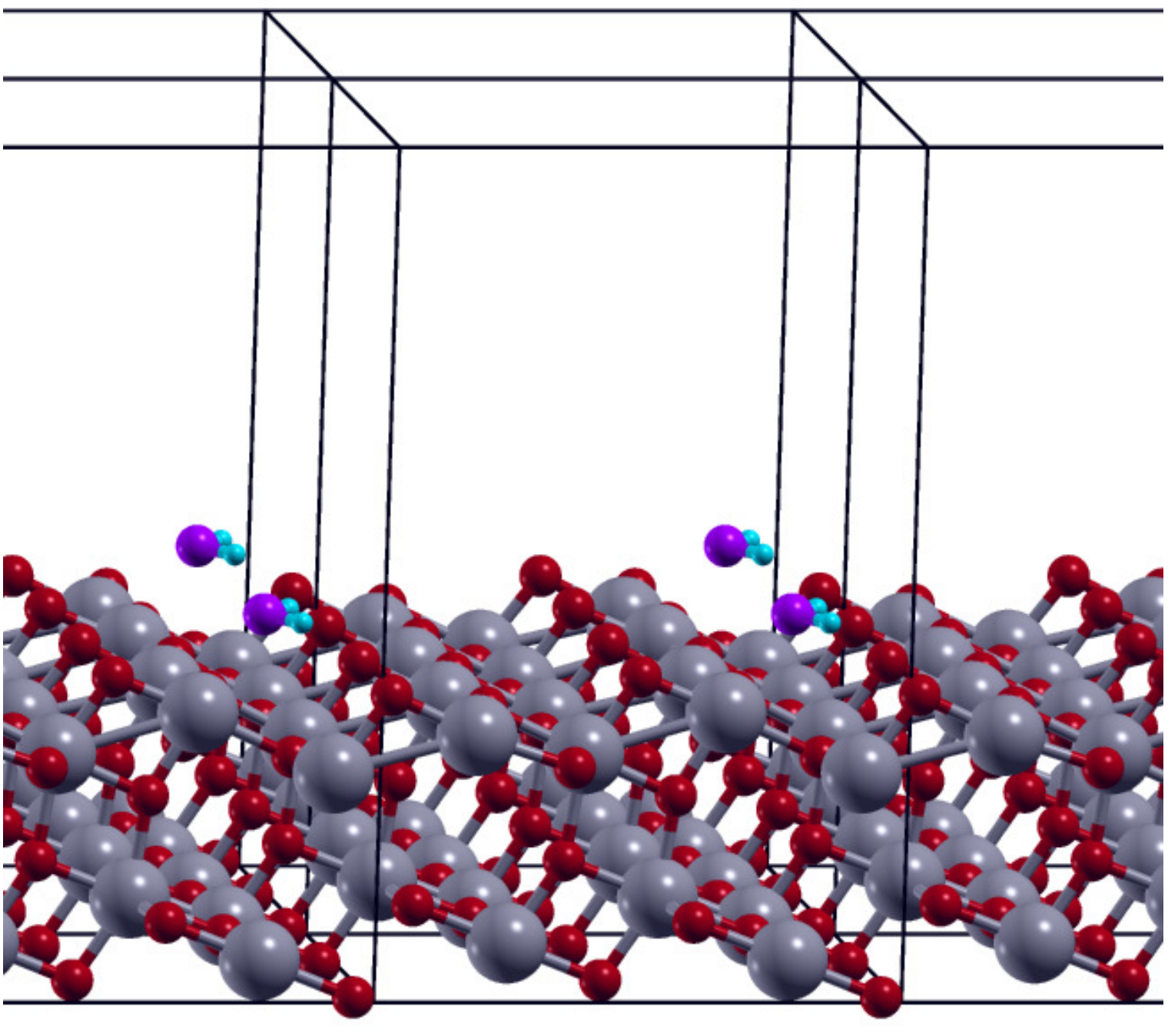

(a) CO @ Anatase(101)

(b) NO @ Anatase(101)

(c) H_2O @ Anatase(101)

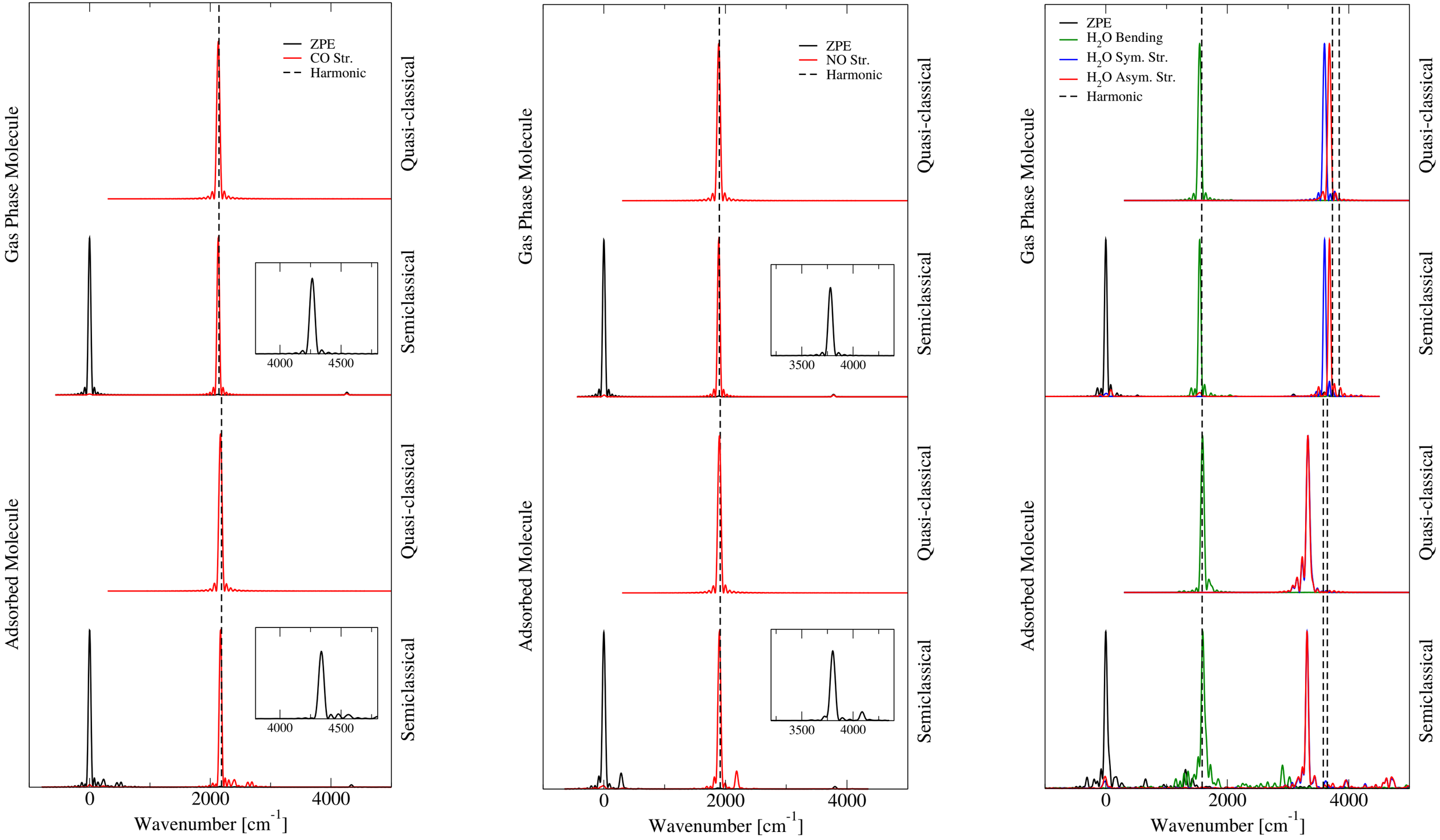

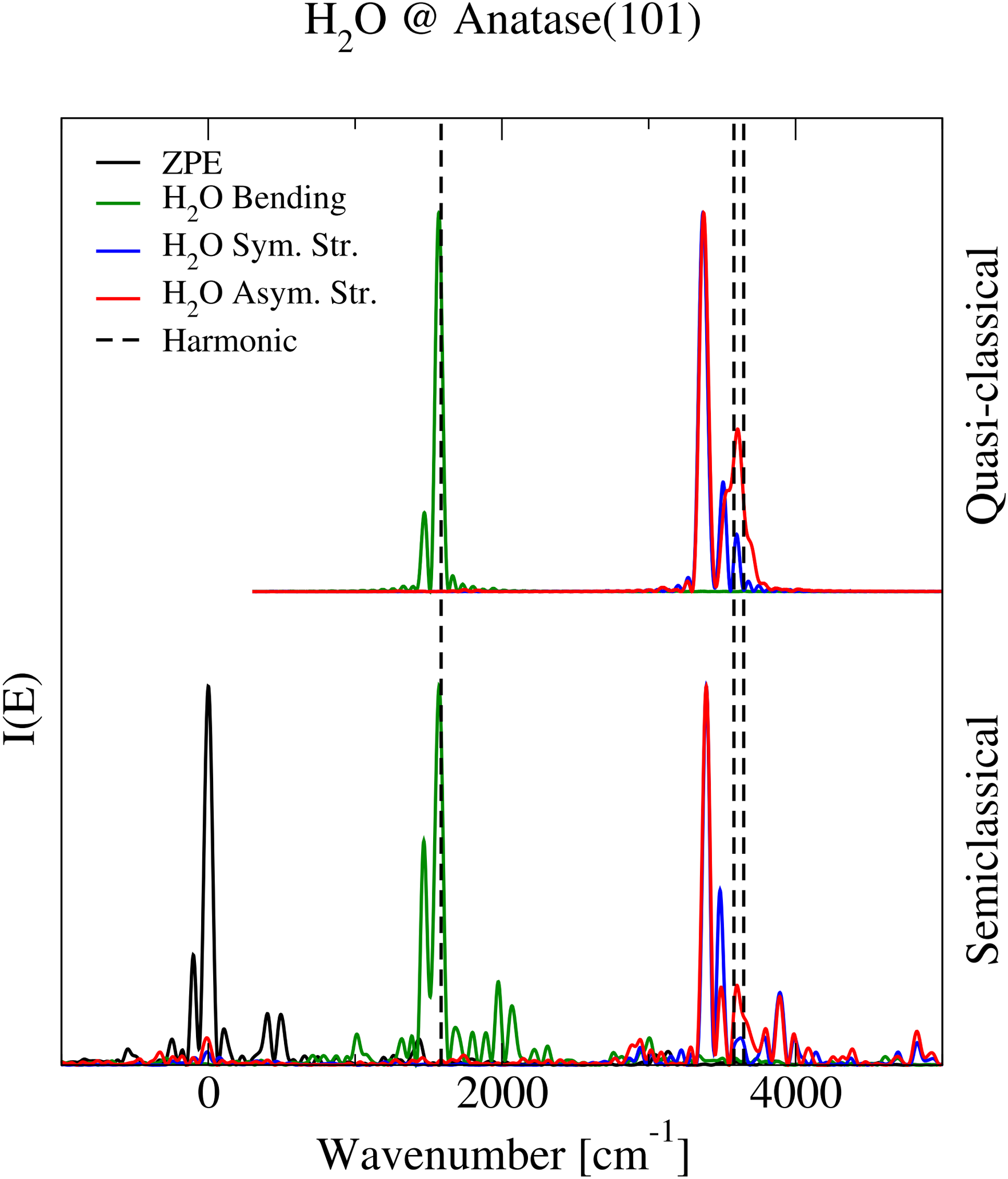
H2O @ Anatase(101)
ZPE
H2O Bending
H2O Sym. Str.
H2O Asym. Str.
Harmonic
Quasi-classical
Semiclassical
I(E)
0
2000
4000
Wavenumber [cm-1]

(a)

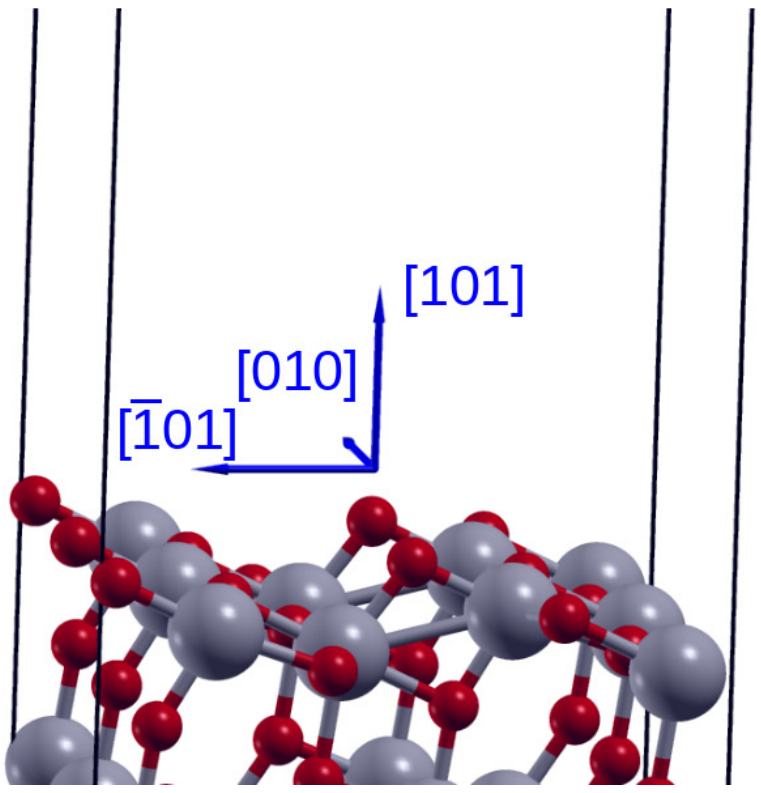

(b) CO @ Anatase(101)

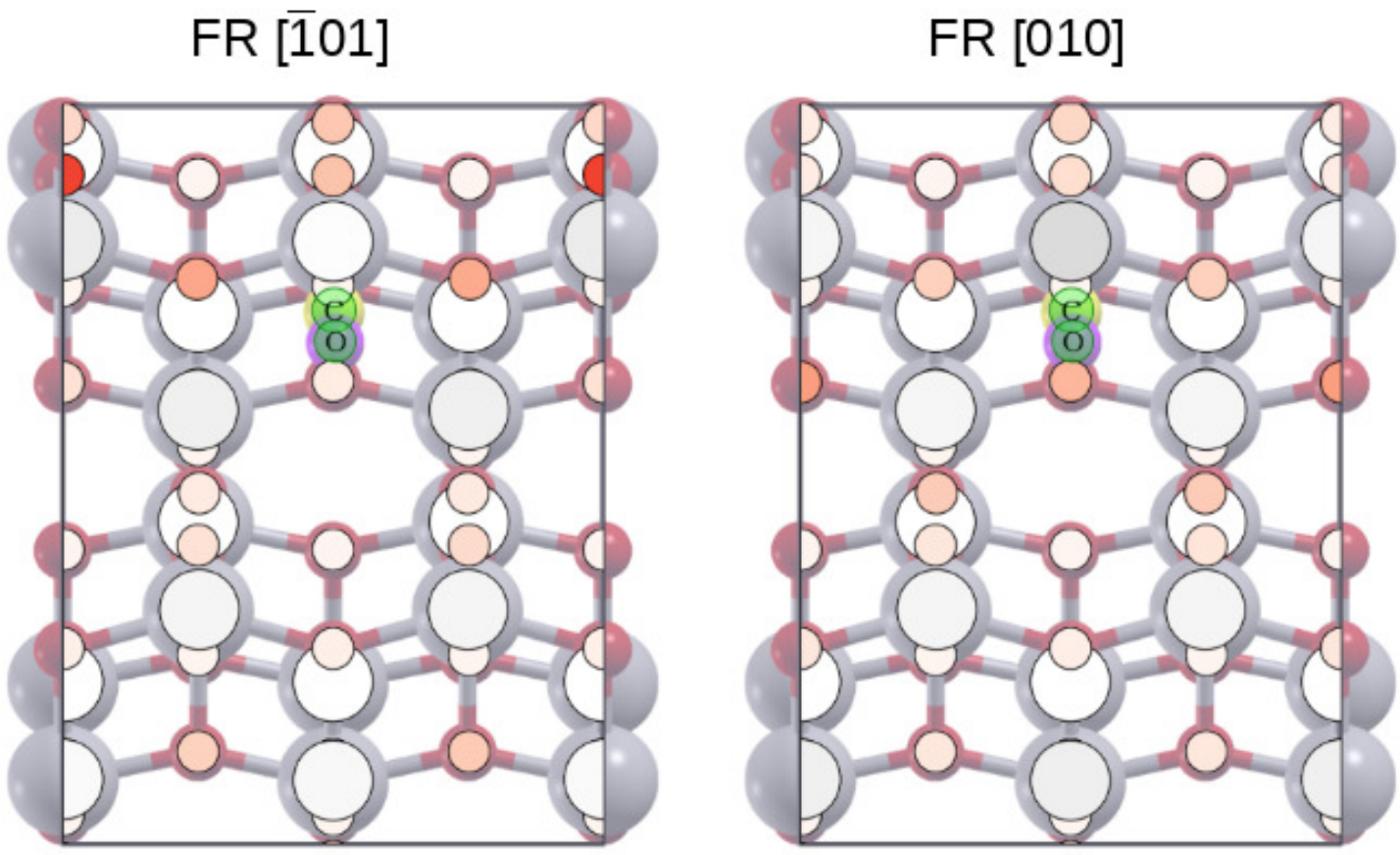

(c) NO @ Anatase(101)

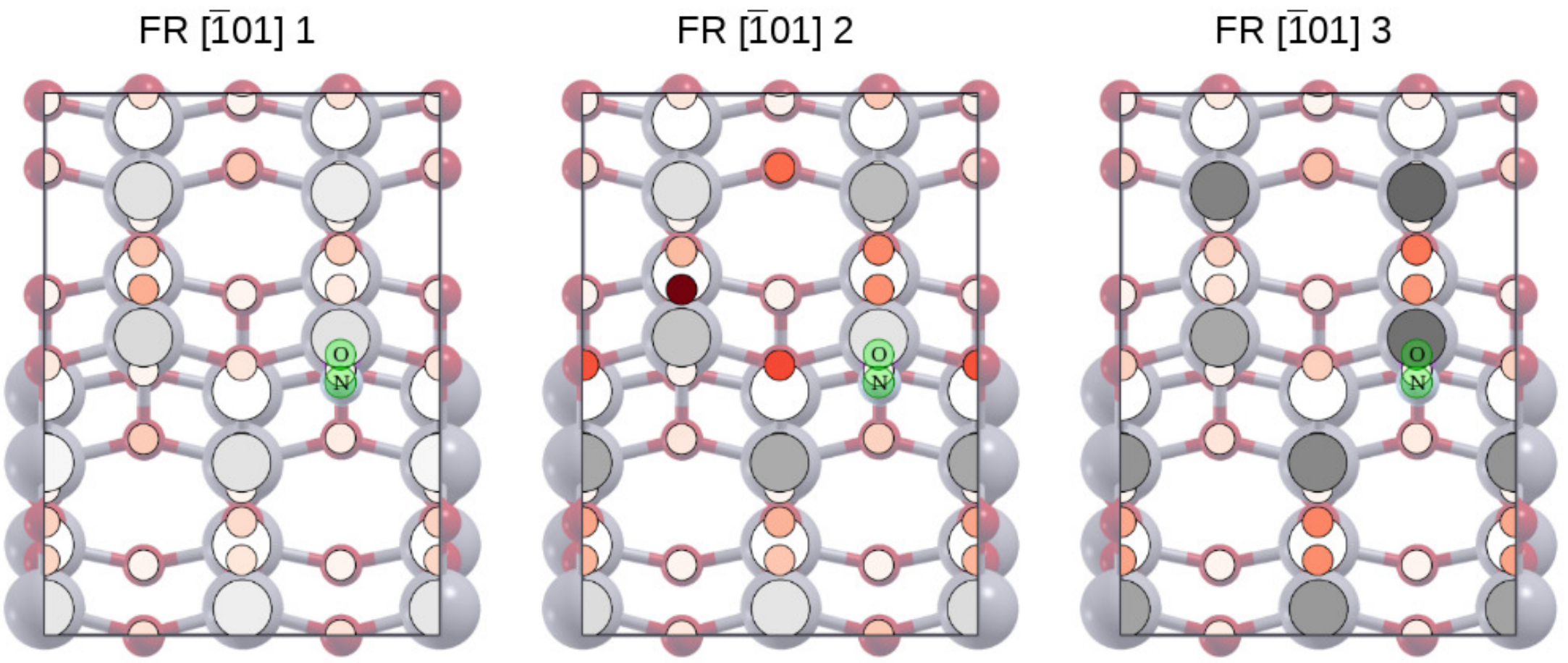

(d) H_2O @ Anatase(101)